scientific reports

OPEN

Palladium anchored to BisPyP@bilayer-SiO$_2$@NMP organic–inorganic hybrid as an efficient and recoverable novel nanocatalyst in suzuki and stille C–C coupling reactions

Eid Ahmed Abdalrazaq[1], Hala Kh. Mohammed[2], Daria K. Voronkova[3,4], Sanjeev Kumar Joshi[5], Ebraheem Abdu Musad Saleh[6], Anaheed Hussein Kareem[7], Abhinav Kumar[8], Ahmed Alawadi[10,11,9], Ali Alslaami[12] & Rohollah Fathollahi[13]✉

The palladium anchored to BisPyP@bilayer-SiO$_2$@NMP organic–inorganic hybrid was employed as an effective and recyclable organometallic catalyst in Suzuki and Stille C–C coupling reactions. The structure of this magnetic nanocatalyst was determined using various techniques such as SEM, TEM, FT-IR, EDS, ICP-OES, VSM, N$_2$ adsorption–desorption isotherms, XRD, and TGA. In both of the mentioned coupling paths, the yields of the products were very favorable and ranged from 90 to 98%. Also, they had significant features compared to previous reports, such as very short reaction time (5–15 and 7–20 min respectively in the Suzuki and Stille reactions), easy work-up, broad substrate scope, ease of separation of the catalyst using a magnet, suitable reproducibility of the catalyst in 6 runs, heterogeneous nature of the catalyst and not washing it during consecutive runs with confirmation of hot filtration and ICP-OES methods.

Creating reusable and environmentally friendly catalytic systems has received a lot of interest in recent years[1–3]. In this context, there is a great deal of interest in a range of chemical reactions related to the immobilization of catalysts on solid materials[4–6]. Nanoparticles, among other solid materials, are suitable supports and play essential roles in the creation of catalysts in terms of recyclability and selectivity[7,8]. Because of their high surface-to-volume ratio, outstanding efficiency, stability, and recoverability, nanomaterials can be used as a bridge between homogeneous and heterogeneous catalysis[9–11]. Iron oxide magnetic nanoparticles, in particular Fe$_3$O$_4$ nanoparticles, have piqued the interest of researchers due to their distinctive features and application possibilities in a variety

[1]Department of Chemistry, Faculty of Science, Al Hussein Bin Talal University, Ma'an, Jordan. [2]Medical Laboratory Techniques Department, Almaarif University College, Ramadi, Iraq. [3]Department of Mathematics and Natural Sciences, Gulf University for Science and Technology, Mishref Campus, Mubarak Al-Abdullah, Kuwait. [4]Bauman Moscow State Technical University Moscow, Moscow, Russia. [5]Department of Mechanical Engineering, Uttaranchal Institute of Technology, Uttaranchal University, Dehradun 248007, India. [6]Department of Chemistry, College of Arts and Science, Prince Sattam Bin Abdulaziz University, 11991 Wadi Al-Dawasir, Saudi Arabia. [7]College of Health and Medical Technology, Al-Ayen University, Thi-Qar 64001, Iraq. [8]Department of Nuclear and Renewable Energy, Ural Federal University Named After the First President of Russia Boris Yeltsin, Ekaterinburg, Russia 620002. [9]College of Technical Engineering, The Islamic University, Najaf, Iraq. [10]College of Technical Engineering, The Islamic University of Al Diwaniyah, Al Diwaniyah, Iraq. [11]College of Technical Engineering, The Islamic University of Babylon, Babylon, Iraq. [12]College of Medical Technique, The Islamic University, Najaf, Iraq. [13]Takin Shimi Sepanta Industries Co, Sirvan Industrial Zone, PO 6958140120, Ilam, Iran. ✉email: rfathollahi_2011@yahoo.com

of areas and sciences[12,13]. The most notable advantage of magnetic nanoparticles is their ease of separation from reaction mixtures using an external magnet, which increases adaptability in work-up operations[14,15].

Mesoporous silica materials, such as SiO_2, on the other hand, have drawn a lot of interest in the domains of adsorption[16], drug delivery systems[17], extraction[18], and particularly catalysis[19]. Their unique qualities, such as their substantial surface area, result in significant loading capacities for catalyst immobilization. Additionally, their large and uniform pore size is appropriate for immobilizing organic ligands and transition metals, and their excellent thermal stability (more than 800 °C) makes them usable in difficult reaction circumstances[20,21]. These characteristics urge scientists to utilize these substances as supports for various catalyst types. For practical applications, the coating of Fe_3O_4 particles with SiO_2 layers to create porous magnetic nanocomposite is of tremendous interest. Because mesoporous magnetic nanocomposites offer the benefits of mesoporous materials (such as large surface area and large pore size) and magnetic nanoparticles (such as easy separation using an external magnet). To achieve excellent selectivity and activity, as well as to facilitate simple catalyst separation and reusability, homogeneous catalysts are immobilized into mesoporous magnetic nanocomposite[20–24]. Solid-state synthesis processes allow for precise control over the size, shape, and morphology of the nanoparticles. This control is crucial in catalysis as the activity and selectivity of a catalyst are often size-dependent[25–27]. Nanocatalysts synthesized using solid-state methods often exhibit enhanced catalytic activity compared to their bulk counterparts. The high surface-to-volume ratio of nanoparticles allows for more active sites, leading to increased catalytic efficiency[25–29]. Supported catalysts on solid substrates are often easier to handle and recover from reaction mixtures. The solid substrate provides mechanical support and facilitates catalyst separation and recycling, making the catalytic process more efficient and cost-effective[25–29].

One of the most significant processes in the synthesis of organic compounds is carbon–carbon cross-coupling reactions[30]. Palladium has been the most widely used transition metal catalyst for various coupling reactions during the last few decades. Although homogeneous palladium catalysts like Pd(OAc)_2 and PdCl_2 have generally high activity, their use has been constrained by their inability to be easily separated from the reaction mixture and recovered, as well as by the considerable environmental damage they cause[31–35]. The creation of heterogeneous palladium catalysts to overcome the aforesaid limitations has important theoretical and practical significance and also is one of the key aims of green chemistry[36–38]. Consequently, to immobilize the palladium catalysts, solid materials such as polymer materials, carbon, zeolite, and various forms of silica (amorphous silica, mesoporous molecular sieves, solids produced by co-condensation of silicate precursors, and many more) have been utilized[39–43].

Carbon–carbon couples have wide-ranging applications across industries such as pharmaceuticals, materials science, and chemical manufacturing. They are employed in drug development to design and synthesize medicinal compounds with specific biological activities[44]. In polymer synthesis, carbon–carbon bonds are vital for determining the strength, flexibility, and other properties of polymers[45,46]. Organic synthesis extensively utilizes carbon–carbon coupling reactions to construct complex organic molecules using cross-coupling reactions. Several carbon–carbon coupling reactions, such as the Suzuki–Miyaura, Stille, Heck, and Negishi reactions, are commonly utilized in chemical manufacturing. These reactions enable the formation of carbon–carbon bonds between different organic fragments, facilitating the assembly of complex molecules required for specific applications[47,48]. Additionally, carbon–carbon composites, comprising carbon fibers within a carbon matrix, are highly robust and lightweight materials used in aerospace and automotive industries for manufacturing aircraft parts and sports car bodies[49,50].

In this scientific article, considering the importance of carbon–carbon couples in different industries, we present the synthesis and characterization of a novel anchored palladium complex on the BisPyP@Bilayer-SiO_2@NMP organic–inorganic hybrid (Pd-BisPyP@bilayer-SiO_2@NMP) as an effectual mesoporous magnetic catalyst for the cross-coupling reactions in the presence of phenylboronic acid and triphenyltin chloride in very short periods under relatively mild conditions.

Experimental
Chemicals and devices
All specifications of raw materials and devices are given in the related files.

Preparation of the catalyst
In order to produce the Pd-BisPyP@bilayer-SiO_2@NMP catalyst, we first created Fe_3O_4 magnetic nanoparticles using the co-precipitation approach and intermediate **I** (xSiO_2@Fe_3O_4) according to prior research[51]. In continuation, in order to synthesize Fe_3O_4 coated with two layers of silica (bilayer-SiO_2@Fe_3O_4), intermediate **I** (0.1 g) was dispersed in a mixed solution of deionized water (80 mL), cetyltrimethylammonium bromide (CTAB, 0.3 g), aqueous ammonia (25 wt%, 1 mL), and ethanol (60 mL) via ultrasonication (25 min). The next step was to mix a suspension containing 0.2 g of intermediate **II**, 1.66 mM of 3-chloropropyltriethoxysilane, and 25 mL of dry toluene solvent under reflux for 24 h. After the end of the reflux time to produce intermediate **III**, the resulting precipitate was filtered and washed with ethanol, toluene and deionized water. The 1,3-bis(4-pyridyl)propane was then immobilized on its surface by stirring a combination of 1,3-bis(4-pyridyl)propane (0.1 g), intermediate **III** (0.3 g), and toluene (25 mL) for 14 h while it was refluxed in an N_2 gas atmosphere (Intermediate **IV**). The final stage involved dispersing Intermediate **IV** (0.5 g) in ethanol and combining it with 0.25 g of palladium acetate that refluxed for 24 h. After that, the NaBH_4 (0.4 mmol) was added to the reaction mixture and stirred for 3 h. The black solid product Pd-BisPyP@bilayer-SiO_2@NMP was obtained by filtration, washed with ethanol and dried in oven at 70 °C (Scheme 1).
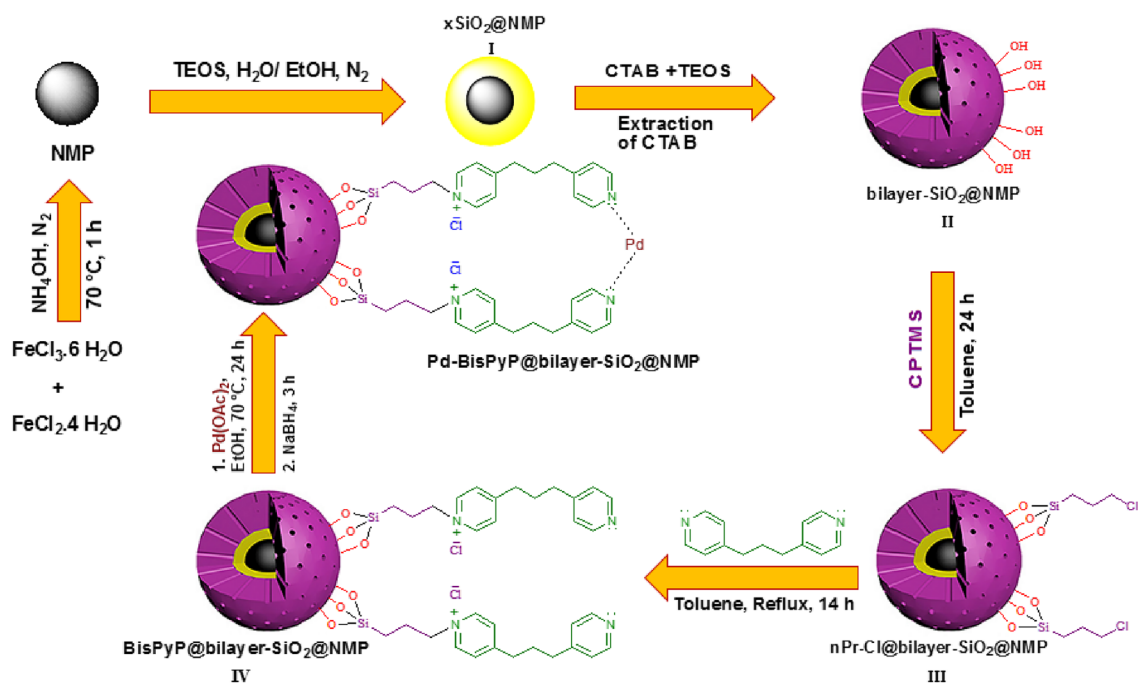
Scheme 1. The synthesis steps Pd–BisPyP@bilayer-SiO$_2$@NMP.

General method for carbon–carbon coupling through Suzuki or Stille reactions

1 mmol aryl halide, 1 mmol phenylboronicacid (or 0.5 mmol triphenyltin chloride), 3 mmol potassium hydroxide and 5 mg Pd-BisPyP@bilayer-SiO$_2$@NMP (1.06 mol%) were stirred in a flask at a temperature of 80 °C in PEG-based solvent (3 mL) until the reaction was completed by TLC monitoring. After the time required to complete the reaction, the catalyst was separated by simple filtration in the vicinity of an external magnetic field. It was cleaned with EtOAc and dried in oven for another run. Next, the organic layer was extracted with diethyl ether (5 mL, four times) from PEG in a separating funnel by help of adding water. Finally, the solvent was evaporated and pure biphenyl derivatives were obtained in excellent yields.

Ethics approval and consent to participate

The author's declare that the paper is not submitted simultaneously to another journal. The submitted work is original and has not been published elsewhere in any form or language, and the authors have no conflict of interest regarding this manuscript. The authors agree to participate in submitting our manuscript to this journal, and agree to the publication of our research data in this journal.

Results and discussion

The successful functionalization of the bare Fe$_3$O$_4$ nanoparticles can be deduced from the FT-IR technique. The FT-IR spectra for NMP (Fe$_3$O$_4$) (i), bilayer-SiO$_2$@NMP (ii), BisPyP@bilayer-SiO$_2$@NMP (iii), and Pd-BisPyP@ bilayer-SiO$_2$@NMP (4), are demonstrated in Fig. 1. In Fig. 1 i, the two peaks at 463 and 574 cm^{-1} are attributed to the vibrations of Fe–O bond[52]. In the FT-IR pattern of bilayer-SiO$_2$@NMP, the coating of bare Fe$_3$O$_4$ nanoparticles with silica layers was confirmed by observing the absorption band related to Si–O–Fe vibration at 950 cm^{-1}[52]. Also, the 803 and 1026 cm^{-1} bands are corresponded to the symmetric and asymmetric vibrations of Si–O–Si in SiO$_2$ (Fig. 1ii)[52]. In Fig. 1iii, the presence of immobilized 3-chloropropyltriethoxysilane (nPr-Cl@ bilayer-SiO$_2$@NMP), and the grafting 1,3-bis(4-pyridyl)propane to intermediate **III** are confirmed via Si–C stretching vibration at 1045 cm^{-1}[53], and C–N stretching vibration at 1380 cm^{-1}, respectively[53]. Additionally, the anchoring of palladium to BisPyP@bilayer-SiO$_2$@NMP was confirmed with a shift of C=N vibration stretching in Pd-BisPyP@bilayer-SiO$_2$@NMP (1660 cm^{-1} in Fig. 1iv), compared to BisPyP@bilayer-SiO$_2$@NMP (1670 cm^{-1} in Fig. 1iii), to a lower frequency which is the reason for this shift is the coordination of Pd to supported BisPyP onto functionalized bilayer-SiO$_2$@NMP[21]. Other adsorptions in the structure of the catalyst are mentioned in Table 1.

SEM was used to analyze the surface morphology of the Pd-BisPyP@bilayer-SiO$_2$@NMP nanocatalyst. Quasi-spherical particles with an average size of 15 to 60 nm can be seen in the SEM image of Pd-BisPyP@bilayer-SiO$_2$@ NMP (Fig. 2).

The study of the TEM images of BisPyP@bilayer-SiO$_2$@NMP (a), and Pd-BisPyP@bilayer-SiO$_2$@NMP (b) depicted in Fig. 3 amply supports the conclusions drawn from the SEM image, because the quasi-spherical shape of the nanoparticles can be clearly seen in these images. In addition, the comparison of these two images shows that the quasi-spherical structure of the substrate nanoparticles has not undergone much change after anchoring palladium on it.

In another study, the structure of the catalyst was reviewed with a high-resolution TEM image (Fig. 4). This image supports the distribution of Pd particles throughout the support, which can be seen as black dots.
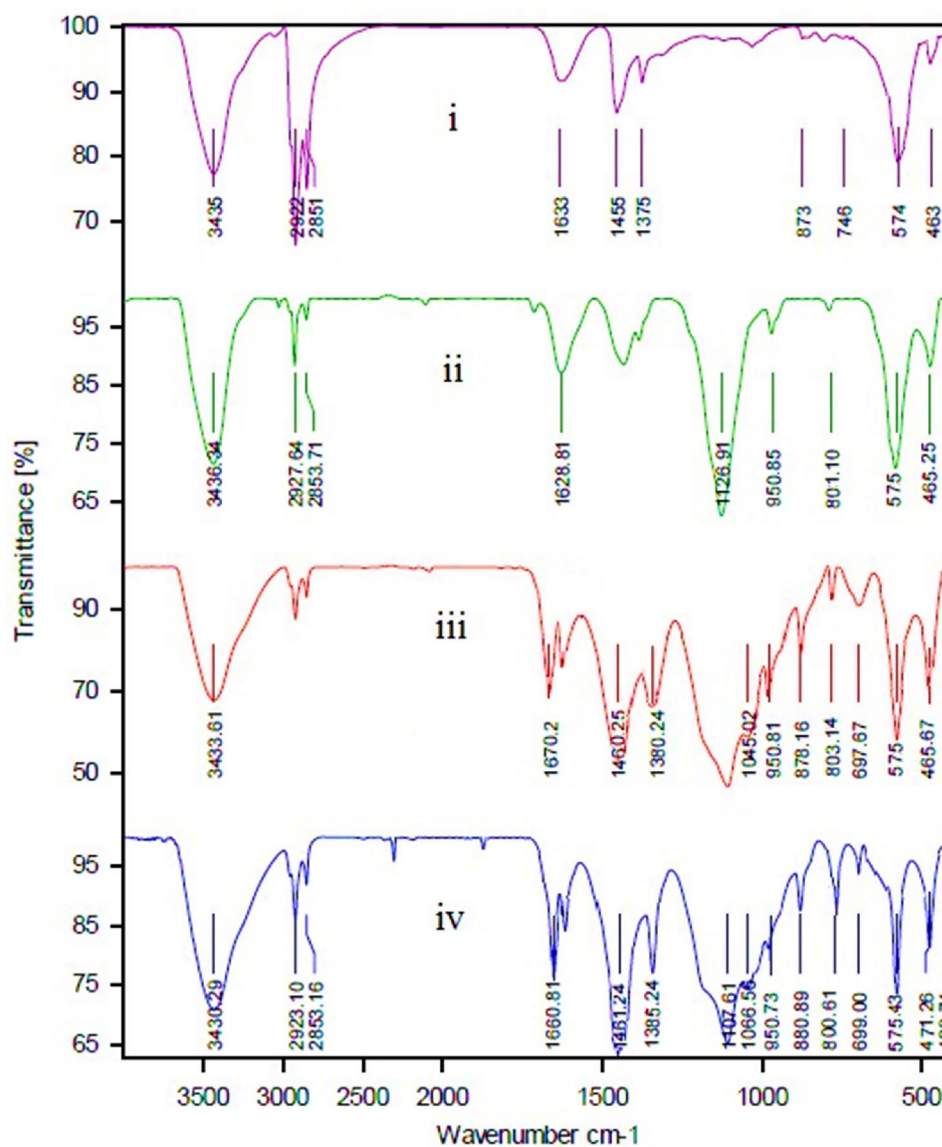
Figure 1. FT-IR spectra of NMP (Fe$_3$O$_4$) (i), bilayer-SiO$_2$@NMP (ii), BisPyP@bilayer-SiO$_2$@NMP (iii), and Pd-BisPyP@bilayer-SiO$_2$@NMP (iv).

Absorption (cm^{-1})	Related bond
574 (i), 575 (ii), 575 (iii), 576 (iv)	Fe–O stretching[52]
803 (ii), 801 (iii), 800 (iv)	Si–O–Si symmetric stretching[52]
950 (ii), 950 (iii), 950 (iv)	Si–O–Fe stretching[52]
1045 (iii), 1066 (iv)	Si–C Stretching[53]
1126 (ii), 1100 (iii), 1107 (iv)	Si–O–Si asymmetric stretching[52]
1380 (iii), 1385(iv)	C–N stretching[53]
1670 (iii), 1660 (iv)	C=N stretching[21]
1460 (iii), 1461 (iv)	C=C stretching[21]
1633 (i), 1628 (ii), ~ 1632 (iii), ~ 1630 (iv)	OH bending on the surface of the SiO$_2$ and Fe$_3$O$_4$[52]
2923 (iii), 2923 (iv)	C–H symmetric stretching[53]
3435 (i), 3436 (ii), 3433 (iii), 3430 (iv)	OH stretching on the surface of the SiO$_2$ and Fe$_3$O$_4$[52,53]

Table 1. FT-IR data of NMP (Fe$_3$O$_4$) (i), bilayer-SiO$_2$@NMP (ii), BisPyP@bilayer-SiO$_2$@NMP (iii), and Pd-BisPyP@bilayer-SiO$_2$@NMP (iv).
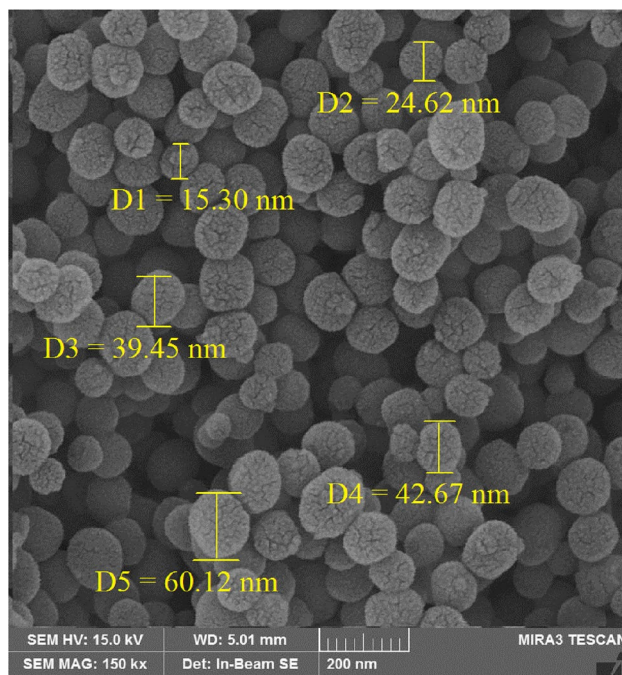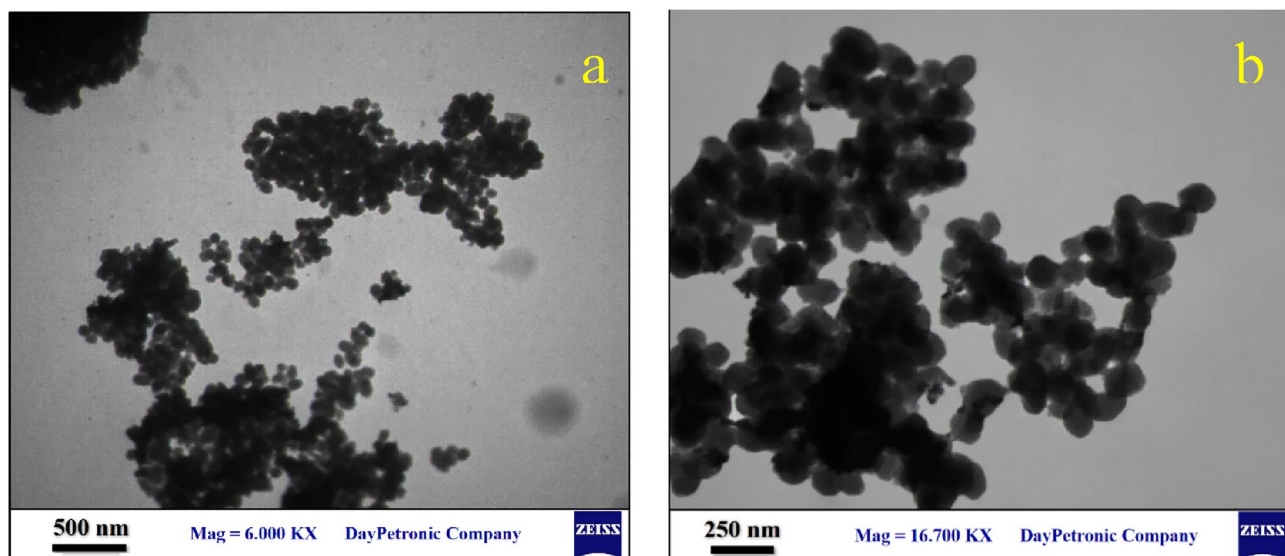
Figure 2. The SEM image of Pd-BisPyP@bilayer-SiO$_2$@NMP.

Figure 3. TEM images of BisPyP@bilayer-SiO$_2$@NMP (**a**), and Pd-BisPyP@bilayer-SiO$_2$@NMP (**b**).

Energy dispersive X-ray spectroscopy analysis, often called EDS, is a practical technique for revealing information on different catalyst elements. Figure 5 confirms the successful fabrication of nanoparticles by showing the presence of C, O, N, Fe, Si, Cl and Pd species in the Pd-BisPyP@bilayer-SiO$_2$@NMP nanocatalyst structure. Meanwhile, the elemental mapping technique images support the presence of all the mentioned constituent elements in the mesoporous skeleton (Fig. 6). It is worth noting, using inductively coupled plasma atomic emission spectroscopy, the precise quantity of palladium in Pd-BisPyP@bilayer-SiO$_2$@NMP was determined to be 2.123×10^{-3} mol g^{-1}.

Magnetic measurement for bare Fe$_3$O$_4$ (a) and Pd-BisPyP@bilayer-SiO$_2$@NMP (b) were carried out, and results are demonstrated in Fig. 7. According to this figure, the saturation magnetic value of catalyst (44.61 emu g^{-1}) is lower than bare Fe$_3$O$_4$ (73.84 emu g^{-1}). This difference could be attributed to the presence of silica layers and the Pd-BisPyP complex attached to the nanoparticle surface. However, by applying an external magnetic field, the catalyst can be rapidly separated from the reaction mixture.

Investigating the porosity of the Pd-BisPyP@bilayer-SiO$_2$@NMP nanocatalyst and its generating components was done using the nitrogen adsorption–desorption technique (Fig. 8). In Table 2, the findings of this
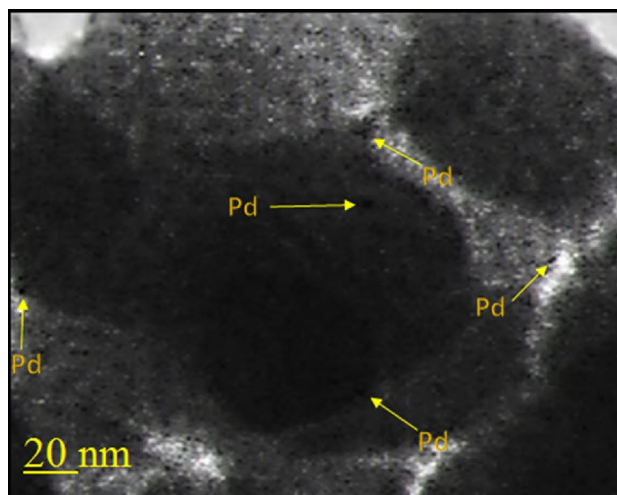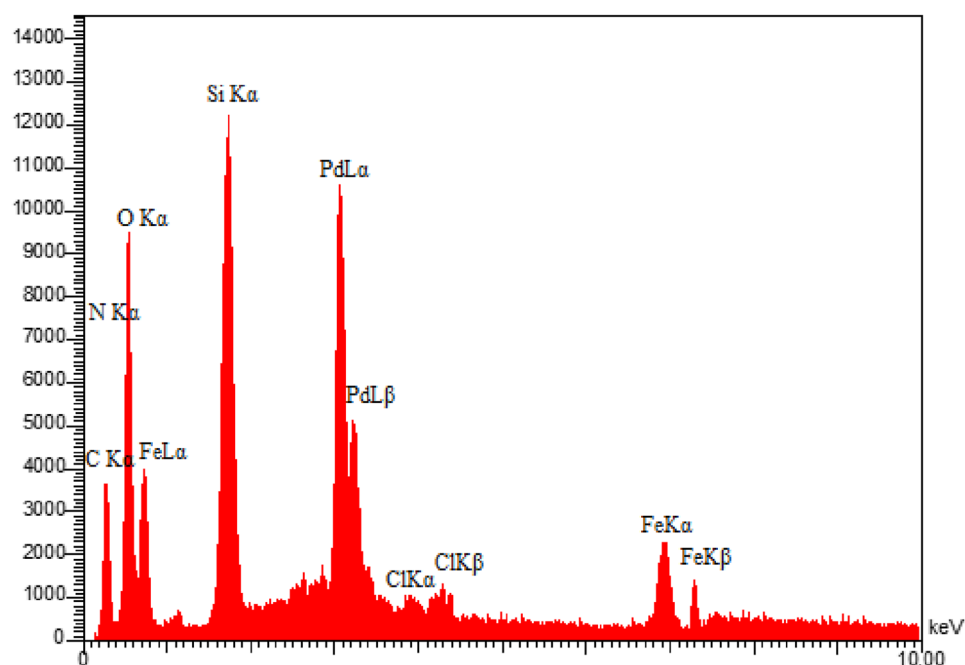
Figure 4. HRTEM image of Pd-BisPyP@bilayer-SiO$_2$@NMP.

Figure 5. The EDS spectrum of Pd-BisPyP@bilayer-SiO$_2$@NMP.

investigation are enumerated. According to the information in this table, Pd-BisPyP@bilayer-SiO$_2$@NMP has a lower specific surface area than BisPyP@bilayer-SiO$_2$@NMP, xSiO$_2$@Fe$_3$O$_4$, and Fe$_3$O$_4$; this is because organic groups and Pd complexes have been anchored on the mesoporous channels of magnetic silica nanoparticles. In addition, the pore size distribution (BJH model) and BET curves of the catalyst are provided in the supplementary material (Figs. S7 and S8, respectively).

Thermal gravimetric analysis (TGA) was used to infer the thermal stability of the produced nanocatalyst and the formation of bonds between the complex and the nanoparticles. Figure 9 displays the TGA curves for bare NMP (green curve), bilayer-SiO$_2$@NMP (blue curve), and the Pd-BisPyP@bilayer-SiO$_2$@NMP (red curve). The TGA diagram of all three samples shows a slight weight loss below 200 °C, which is caused by the removal of surface hydroxyl groups and physically absorbed solvents. The TGA curve of Pd-BisPyP@bilayer-SiO$_2$@NMP showed two other stages of weight loss in addition to the preliminary weight loss (3.09% weight loss at temperature below 200 °C): (i) 10.72% weight loss in the temperature range of 200–380 °C (arising from decomposition of organic moieties of the complex), and (ii) 9.83% decrease weight between 380 and 700 °C (due to the decomposition of silanol groups)[54]. The above observations confirmed the thermal stability of the catalyst and the immobilization of the palladium complex on the bilayer-SiO$_2$@NMP.
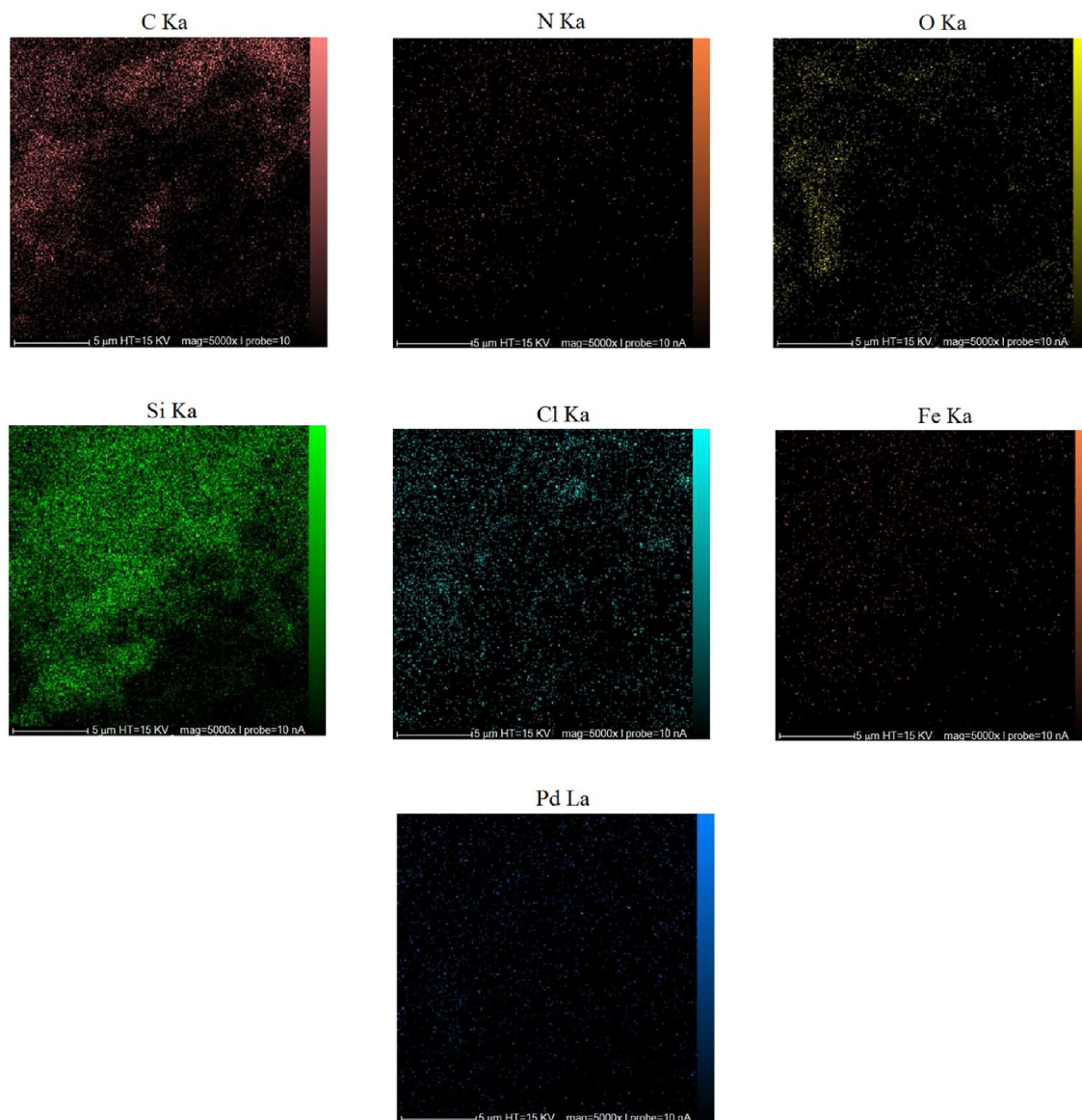
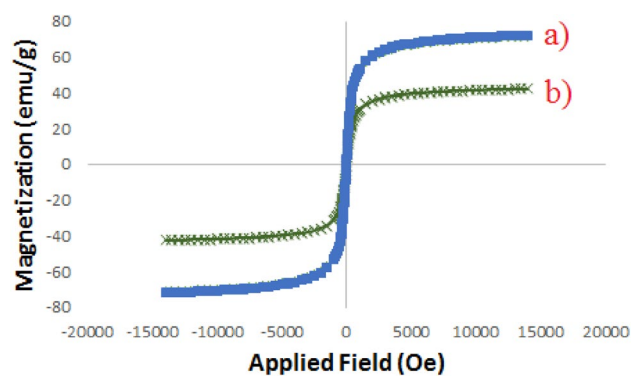**Figure 6.** The elemental mapping images of Pd-BisPyP@bilayer-SiO$_2$@NMP.

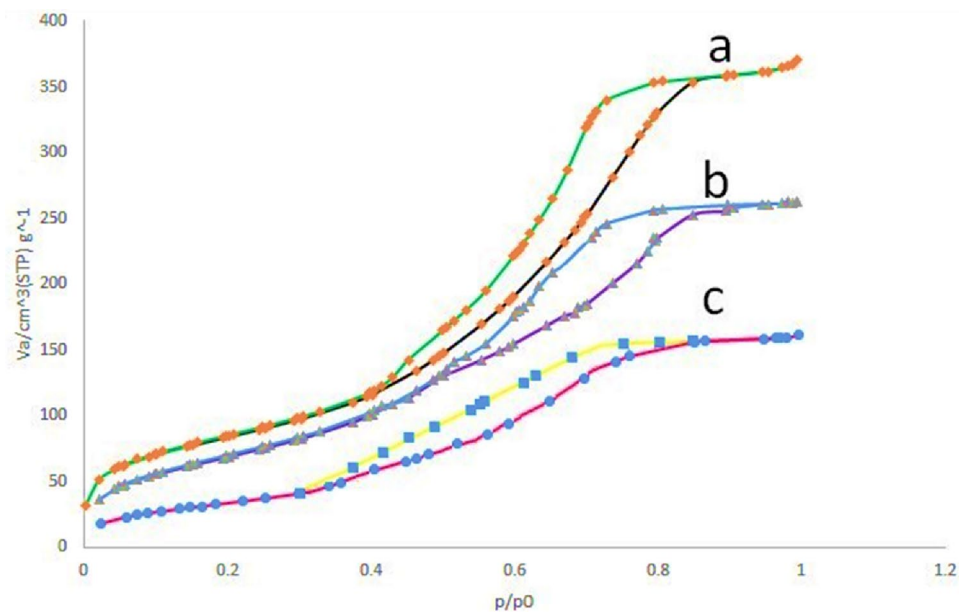**Figure 7.** Magnetization curves for Fe$_3$O$_4$ (**a**), and Pd-BisPyP@bilayer-SiO$_2$@NMP (**b**).

Figure 8. Nitrogen adsorption–desorption isotherms of $xSiO_2@Fe_3O_4$ (**a**), BisPyP@bilayer-SiO_2@NMP (**b**), and Pd-BisPyP@bilayer-SiO_2@NMP (**c**).

Sample	SBET (m²/g)	$r_{p,peak}$ by BJH method (nm)ᵃ	Pore vol (cm³/g)	Ref
Fe_3O_4	480.0	1.254	0.803	[51]
$xSiO_2@Fe_3O_4$	463.3	1.551	0.779	–
BisPyP@bilayer-SiO_2@NMP	410.9	1.883	0.722	–
Pd-BisPyP@bilayer-SiO_2@NMP	327.7	2.088	0.645	–

Table 2. Texture properties of Pd-BisPyP@bilayer-SiO_2@NMP. ᵃ$r_{p,peak}$: Mean pore radius.
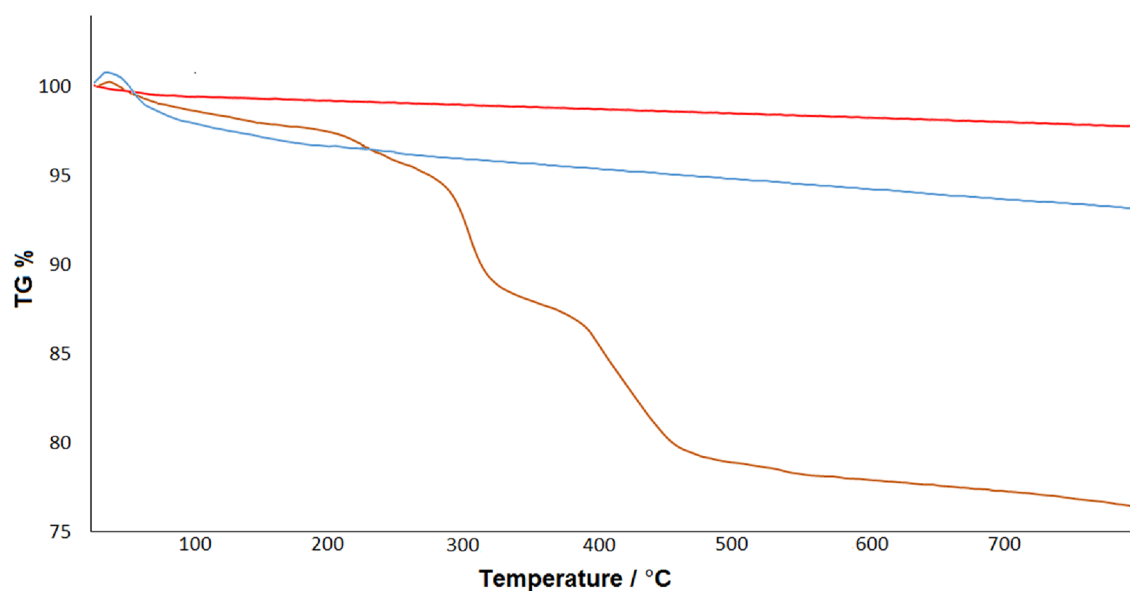

Figure 9. TGA curves of bare NMP (red curve), bilayer-SiO_2@NMP (blue curve), and Pd-BisPyP@bilayer-SiO_2@NMP (green curve).

The structural characteristics of bare NMP (crimson pattern), and Pd-BisPyP@bilayer-SiO$_2$@NMP (blue pattern) were investigated using the XRD method in Fig. 10. The XRD pattern of these two samples, which consists of many peaks at 2θ = 30.66° (220), 34.50° (311), 43.33° (400), 52.66° (422), 56.11° (511) and 62.02° (440), which are related to the crystallographic faces of Fe$_3$O$_4$ particles[55]. Furthermore, the existence of Pd in the catalyst structure was confirmed by the Bragg angles at = 40.01° (111), 46.29° (200), and 68.01° (220) (blue pattern)[56]. It is worth noting that the broad peak at 2θ = 20–30°, and also the peaks observed at 2θ = 18.01°, 48.65°, 49.33°, 37.33° and 38.41° indicate the presence of amorphous silica around the Fe$_3$O$_4$ particles and the crystalline nature of the catalyst, respectively[54].

Examine of the catalytic property

The catalytic performance of Pd-BisPyP@bilayer-SiO$_2$@NMP in the C–C cross-coupling reaction of aryl halides with phenylboronic acid and triphenyltin chloride was carefully studied. In this regard, to determine the optimize conditions, the reaction between iodobenzene and phenylboronic acid was chosen as a model, and the effect of various factors, including temperature, amount of catalyst, solvent, and base on it was monitored. The results are shown in Table 3. In the first step, the effect of the nature of the solvent on the reaction of the model was studied. The results showed that the type of solvent used has a significant impact on the progress of the reaction, so that no product was observed in 1,4-dioxane (Table 3, entry 1), and small amounts of the product were obtained in H$_2$O and EtOH in the presence of 5 mg of catalyst (Table 3, entries 2 and 3). However, in solvents such as DMF (dimethylformamide) and DMSO (dimethyl sulfoxide), the corresponding biphenyl product was isolated with 69 and 72 yields, respectively (Table 3, entries 4 and 5), and the highest yield was observed in PEG-400 solvent (Table 3, entry 6). Therefore, the PEG-400 solvent was chosen as the most suitable solvent for the mentioned reaction. In the second step, we studied the effect of different bases on the model's reaction. These bases included organic bases (DMAP, Et$_3$N), monobasic (KOH, NaOH), dibasic (Na$_2$CO$_3$), and NaHCO$_3$ (Table 3, entries 6–11). The results showed that Na$_2$CO$_3$ can be a highly effective base for the Suzuki cross-coupling reaction (Table 3, entry 6). Also, KOH and NaOH, despite being stronger bases than Na$_2$CO$_3$ based on their known K$_b$ values, ultimately did not lead to a significant yield of the product, because according to the studies of Knecht and his colleagues[57], for monobasic systems (KOH, NaOH), the amount of free and active hydroxide compared to Na$_2$CO$_3$ and NaHCO$_3$ is more, and this causes their strong combination with palladium species and decrease in biphenyl efficiency for cross-coupling reaction. Also, the reason for the ineffectiveness of organic bases such as Et$_3$N and DMAP is their weak play power. The result of this study, as well as the failure to perform the reaction in the absence of base (Table 3, entry 12), proved that an average basic capacity is necessary to carry out the mentioned reaction using Pd-BisPyP@bilayer-SiO$_2$@NMP. In the third step, our studies were focused on the effect of temperature on the progress of the reaction (Table 3, entries 6 and 13–15). Examining the result of the model reaction in the temperature range of 25 to 90 °C reflected the fact that the reaction is sensitive to temperature, so that a higher temperature can shorten the reaction time and cause a better progress of the reaction. Further investigations showed that the best temperature for the reaction progress is 70 °C (Table 3, entry 6). In the fourth step, the impact of the amount of phenylboronic acid on the performance was also studied (Fig. 11). The reactions performed in the presence of 0.7, 0.8, 0.9, and 1.0 mmol of phenylboronic acid provide 61, 79, 86,
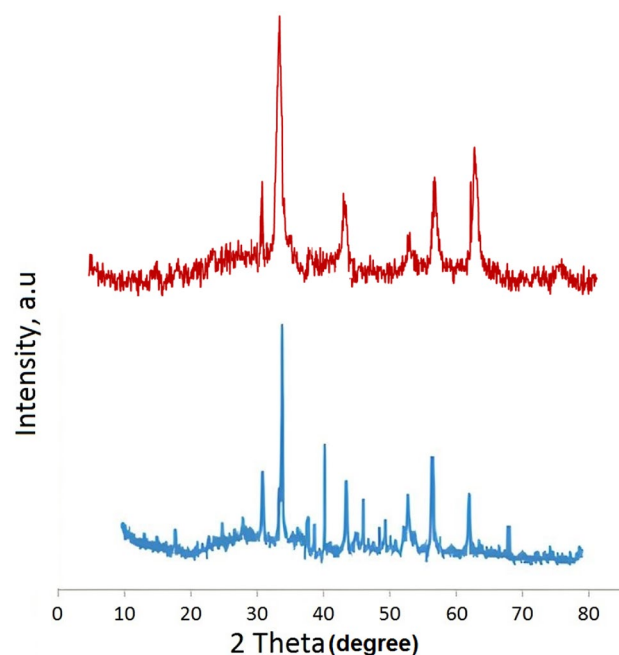

Figure 10. XRD patterns of bare NMP (crimson pattern), and Pd-BisPyP@bilayer-SiO$_2$@NMP (blue pattern).

Entry	Solvent	Base (mmol)	Temperature (°C)	Catalyst (mg)	Time (min)	Yield (%)[b]
1	1,4-Dioxane	Na_2CO_3	70	5	5	–
2	EtOH	Na_2CO_3	Reflux	5	5	26
3	H2O	Na_2CO_3	70	5	5	22
4	DMSO	Na_2CO_3	70	5	5	69
5	DMF	Na_2CO_3	70	5	5	72
6	PEG	Na_2CO_3	70	5	5	98
7	PEG	Et_3N	70	5	5	24
8	PEG	DMAP	70	5	5	27
9	PEG	KOH	70	5	5	64
10	PEG	NaOH	70	5	5	47
11	PEG	$NaHCO_3$	70	5	5	85
12	PEG	–	70	5	240	—
13	PEG	Na_2CO_3	25	5	180	—
14	PEG	Na_2CO_3	50	5	60	57
15	PEG	Na_2CO_3	90	5	5	98
16	PEG	Na_2CO_3	70	4	60	79
17	PEG	Na_2CO_3	70	6	5	98
18	PEG	Na_2CO_3	70	–	1440	–

Table 3. C–C coupling of iodobenzene with phenylboronic acid in the presence of Pd-BisPyP@bilayer-SiO$_2$@ NMP under various conditions[a]. [a]Reaction conditions: iodobenzene (1 mmol), phenylboronic acid (1 mmol), base (3 mmol), solvent (2 mL). [b]Isolated yield.
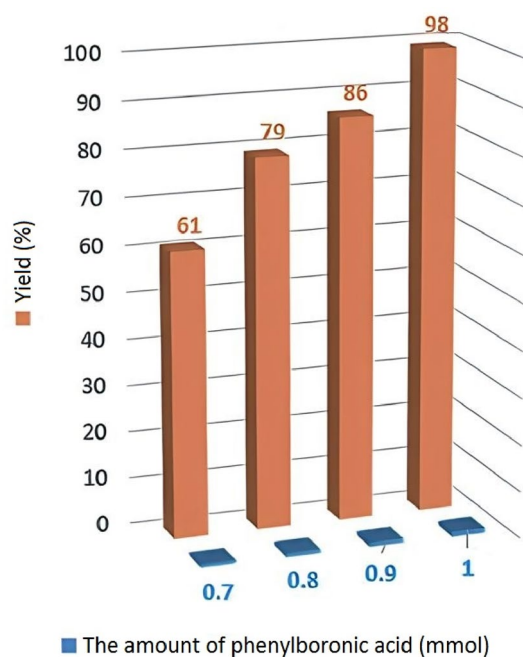

Figure 11. Effect of amount of phenylboronic acid on the efficiency of the model reaction.

and 98 isolated yields, respectively. It has been determined that 1 mmol of phenylboronic acid with 1 mmol of iodobenzene are the optimal amounts to complete the reaction. In the last step, the model reaction was checked with quantities of 4, 5 and 6 mg of Pd-BisPyP@bilayer-SiO$_2$@NMP because the coupling reaction does not occur under catalyst-free conditions (Table 3, entry 18). It was found that 5 mg of BisPyP@bilayer-SiO$_2$@NMP is the optimal amount (Table 3, entry 6), while reducing the amount of catalyst to 4 mg in 60 min resulted in lower efficiency (Table 3, entry 16), increasing the amount of its catalyst to 6 mg did not show superiority over the optimal state (Table 3, entry 17).

After determining the best conditions for the coupling of iodobenzene with phenylboronic acid, in another study this reaction was carried out in the presence of the catalyst parents, i.e. NMP (Fe$_3$O$_4$) (Table 4, entry 1), bilayer-SiO$_2$@NMP (Table 4, entry 2), BisPyP@bilayer-SiO$_2$@NMP (Table 4, entry 3), and also Pd-BisPyP@ xSiO$_2$@NMP (The only difference of this catalyst compared to Pd-BisPyP@bilayer-SiO$_2$@NMP is the use of a silica layer (not two layers) around Fe$_3$O$_4$) (Table 4, entry 4). Subsequently, the amount of palladium in the Pd-BisPyP@bilayer-SiO$_2$@NMP and Pd-BisPyP@xSiO$_2$@NMP measured via the ICP technique, which was equal to 2.123×10^{-3} and 1.112×10^{-3} mol g^{-1}, respectively. Experimental evidence from the ICP technique and Table 4 demonstrated that trick of utilizing two layers of SiO$_2$ on NMP, and also anchoring palladium on the BisPyP@ bilayer-SiO$_2$@NMP was effective for the better progress of the reaction, because the reaction failed in the presence of the catalyst's parents (Table 4, entries 1–3), and only when they connect to each other and form the catalyst, a strong synergistic effect of the catalyst is observed. Immobilization of two layers of SiO$_2$ on NMP leads to the bonding of organic groups to the surface of the substrate, and this causes more palladium to enter the mesoporous channels, and complete the reaction with less amount of catalyst. Besides, the use of double-layer silica prevents the aggregation of magnetic nanoparticles.

To find out the scope of the catalytic system under examination, cross-coupling of phenylboronic acid with diverse aryl halides was tested. The results showed that all reactions proceed at high speed to obtain the corresponding biphenyl derivative with excellent efficiency (Table 5). The electron-donating or electron-withdrawing properties of the substituents do not seem to have a significant effect on the product yield. Also, Aryl bromides and aryl iodides provide better results than aryl chlorides.

For the Stille reaction, the Pd-BisPyP@bilayer-SiO$_2$@NMP catalyst also displays a high activity in PEG-400 solvent through 0.5 mmol of triphenyltin chloride (Ph$_3$SnCl). As the data in Table 6 reflect, the results are similar to those related to the Suzuki reaction.

To demonstrate the selectivity of our catalyst in both Suzuki and Stille coupling methods, 1-bromo-4-chorobenzene was coupled with PhB(OH)$_2$ and Ph$_3$SnCl (Table 5 Entry 15 and Table 6 Entry 10, respectively). The results showed that the coupling occurs only with the bromo functional group, meaning the chloro functional group remains intact during both cross-coupling reactions (Scheme 2).

Scheme 3 shows the catalytic cycle of the Suzuki reaction in the presence of Pd-BisPyP@bilayer-SiO$_2$@NMP catalyst in the following 3 steps, which is supported by the literature[65]: (1) the oxidative addition of Pd to Ar-X (aryl halide), and formation of organopalladium **VI** in the vicinity of Na$_2$CO$_3$ (2) the transmetallation of **VI** gives intermediate **VII** in the presence of phenylboronic acid, and finally (3) product formation and regeneration of palladium catalyst (**V**) by reductive elimination of intermediate **VII**.
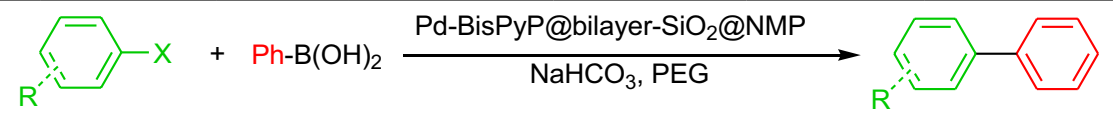
Reusability of catalyst

It is critical to recover and reuse catalysts in green catalytic processes for economic and environmental reasons. As a consequence, the reusability of Pd-BisPyP@bilayer-SiO$_2$@NMP was investigated in the coupling of iodobenzene with phenylboronic acid, and the findings are shown in Fig. 12. After the completion of the reaction, the catalyst was separated using an external magnet and washed with ethyl acetate to extract the product for this investigation. The recovered catalyst was reused up to six times without losing substantial catalytic activity. The average isolated yield for six consecutive cycles is 96%, indicating that this catalyst is recyclable.

Catalyst leaching study

ICP-OES and hot filtration tests were used to investigate palladium leaching from Pd-BisPyP@bilayer-SiO$_2$@NMP. The quantity of palladium in the fresh and reused catalysts was 2.123×10^{-3} mol g^{-1} and 2.109×10^{-3} mol g^{-1}, respectively, according to ICP-OES analysis, indicating that palladium leaching of this catalyst is insignificant. A hot filtration test for the coupling of iodobenzene with phenylboronic acid was explored to assess the stability and heterogeneous nature of Pd-BisPyP@bilayer-SiO$_2$@NMP under the reaction circumstances. In this investigation, 67% of the product was produced in half the reaction duration (the reaction time is 5 min). The reaction
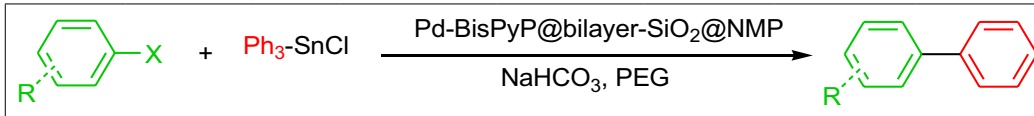
Entry	Catalyst	Yield (%)^a
1	NMP (Fe$_3$O$_4$)	–^{b}
2	bilayer-SiO$_2$@NMP	–^{b}
3	BisPyP@bilayer-SiO$_2$@NMP	–^{b}
4	Pd-BisPyP@xSiO$_2$@NMP	73

Table 4. Investigating the influence of NMP, bilayer-SiO$_2$@NMP, BisPyP@bilayer-SiO$_2$@NMP, and Pd-BisPyP@xSiO$_2$@NMP in the coupling of iodobenzene with phenylboronic acid as a model compound under optimized conditions. ^{a}Isolated yield under optimized conditions. ^{b}No reaction.

| Entry	R	X	Time (min)	Yield (%)[b]	M.p. (°C)		TOF (min^{-1})[c]
					Found	Reported	
1	H	I	5	98	68–70	68–70[58]	18.490
2	4-OCH$_3$	I	8	95	87–89	88–90[58]	11.202
3	4-CH$_3$	I	6	97	45–47	44–46[58]	15.251
4	2-CO$_2$H	I	11	97	107–109	107–109[59]	8.319
5	H	Br	7	96	68–70	68–70[58]	12.938
6	4-CH$_3$	Br	9	98	45–47	44–46[58]	10.272
7	4-OH	Br	10	98	161–163	163–164[60]	9.245
8	4-CHO	Br	12	97	55–57	54–56[61]	7.265
9	4-CN	Br	13	97	84–86	85–86[60]	7.039
10	4-CO$_2$H	Br	13	94	226–228	224–228[62]	6.821
11	4-NO$_2$	Br	9	97	111–113	112–114[58]	10.167
12	4-NH$_2$	Br	10	97	51–53	50–53[61]	9.150
13	4-SH	Br	11	95	109–111	110–111[63]	8.147
14	3-CHO	Br	10	94	52–54	53–54[64]	8.867
15	4-Cl	Br	10	95	71–73	71–73[65]	8.962
16	H	Cl	15	94	162–164	163–164[60]	5.911

Table 5. Preparation of biphenyl derivative from Suzuki reaction using Pd-BisPyP@bilayer-SiO$_2$@NMP[a]. [a]Reaction conditions: aryl halide (1 mmol), PhB(OH)$_2$ (1 mmol), base (3 mmol), Pd-BisPyP@bilayer-SiO$_2$@NMP (5 mg, 1.06 mol%), PEG-400 (2 mL). [b]Isolated yield. [c]Turnover frequency.


Entry	R	X	Time (min)	Yield (%)[b]	M.p. (°C)		TOF (min^{-1})[c]
					Found	Reported	
1	H	I	7	98	68–70	68–70[58]	13.207
2	4-OCH$_3$	I	9	92	87–89	88–90[58]	9.643
3	4-CH$_3$	I	10	97	45–47	44–46[58]	9.150
4	H	Br	8	98	68–70	68–70[58]	11.556
5	4-CH$_3$	Br	14	97	45–47	44–46[58]	6.536
6	4-OH	Br	10	96	161–163	163–164[60]	9.056
7	4-CHO	Br	18	93	55–57	54–56[61]	4.874
8	4-CN	Br	11	98	84–86	85–86[60]	8.404
9	H	Cl	20	90	162–164	163–164[60]	4.245
10	4-Cl	Br	12	90	71–73	71–73[65]	7.075

Table 6. Preparation of biphenyl derivative from Stille reaction using Pd-BisPyP@bilayer-SiO$_2$@NMP[a]. [a]Reaction conditions: aryl halide (1 mmol), Ph$_3$SnCl (0.5 mmol), base (3 mmol), Pd-BisPyP@bilayer-SiO$_2$@NMP (5 mg, 1.06 mol%), PEG-400 (2 mL). [b]Isolated yield. [c]Turnover frequency.

was then repeated, and at halftime, the catalyst was separated, and the filtrated solution was allowed to complete the reaction without a catalyst for another 2.5 min. After that, only 69% of biphenyl was recovered as a product. These trials show that palladium leaching did not occur[66].
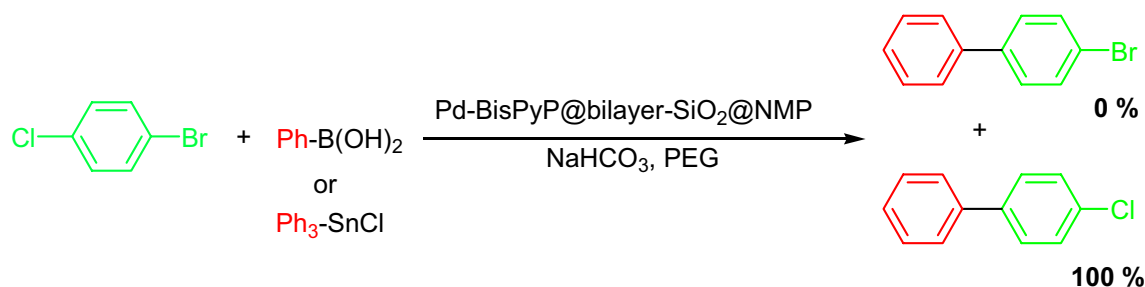
Scheme 2. Selective coupling of 1-bromo-4-chorobenzene with phenylboronic acid in the presence of Pd-BisPyP@bilayer-SiO$_2$@NMP.
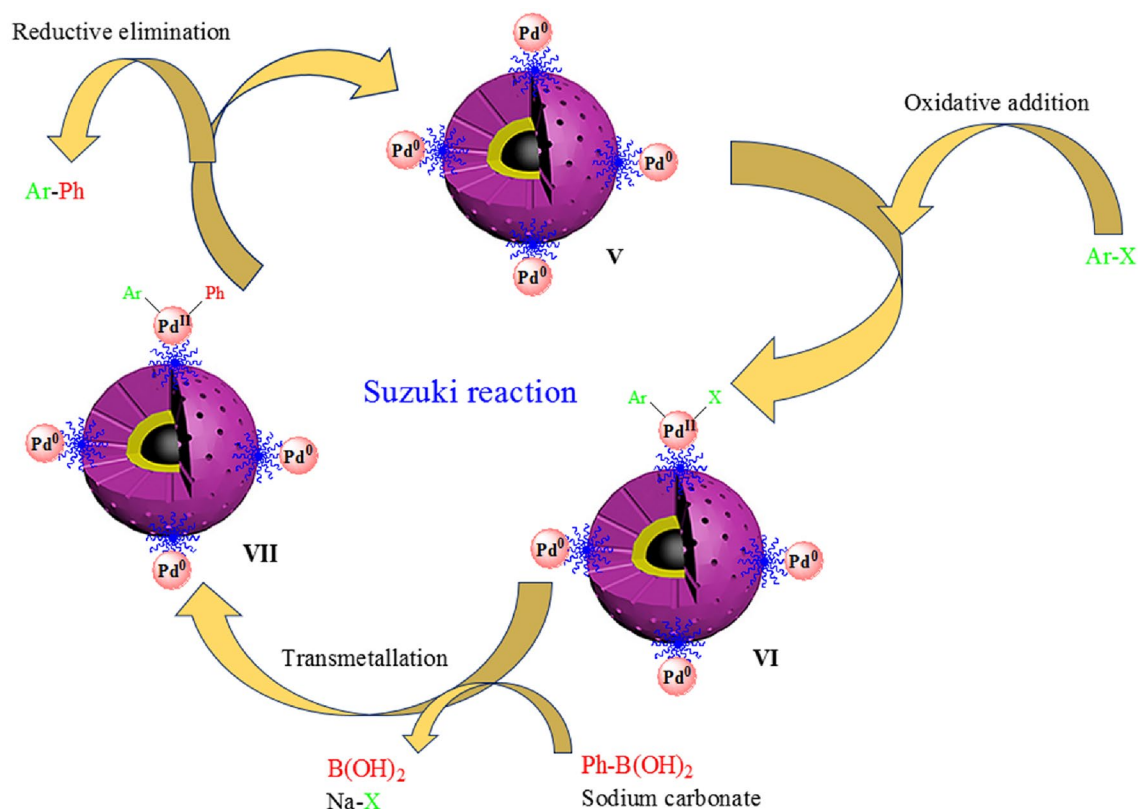
Scheme 3. The suggested catalytic cycle of Suzuki reaction in the presence of Pd-BisPyP@bilayer-SiO$_2$@NMP.

Comparison of the catalyst

The efficiency of Pd-BisPyP@bilayer-SiO$_2$@NMP as a catalyst was demonstrated by comparing it with the catalysts reported in the literature. Results for the coupling of iodobenzene with phenylboronic acid in the presence of Pd-BisPyP@bilayer-SiO$_2$@NMP and previously reported catalysts are summarized in Table 7. In this comparison, various parameters such as reaction condition, reaction times and yields were compared. As shown in Table 7, Pd-BisPyP@bilayer-SiO$_2$@NMP showed high effectivity than other catalysts in terms of reaction time and isolated yield.

Conclusions

In this research, we have presented a new organic–metallic nanocatalyst (Pd-BisPyP@bilayer-SiO$_2$@NMP) with three unique characteristics, i.e., excellent performance in accelerating the reaction time, magnetic nature, and high porosity. These three properties make this magnetic mesoporous material a versatile and effectual catalyst. The catalytic performance of this catalyst was investigated in Suzuki and Stille cross-coupling reactions. These reactions were carried out in eco-friendly conditions and decorated with the following benefits: high purity of products without generation of side products, simple separation of products and catalyst from each other, the phosphine-free structure of the catalyst, the possibility of recovering and reusing the catalyst up to 6 times, high efficiency under relatively moderate conditions, the use of PEG as a green solvent, and not leaching the catalyst, especially the metal parts (Pd), with the confirmation of hot filtration and ICP-OES methods.
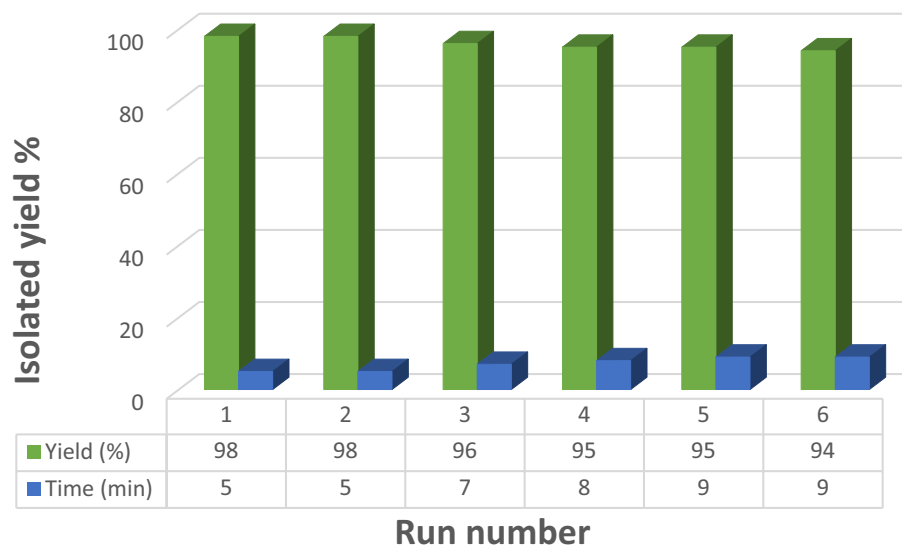
	1	2	3	4	5	6
Yield (%)	98	98	96	95	95	94
Time (min)	5	5	7	8	9	9

Figure 12. The recycling experiment of Pd-BisPyP@bilayer-SiO$_2$@NMP in the coupling of iodobenzene with phenylboronic acid (Suzuki reaction).

Catalyst	Conditions	Time (min)	Yield (%)	References
Mag-IL-Pd	K$_2$CO$_3$, H$_2$O, 60 °C	360	95	[67]
Guanidine/Pd(OAc)$_2$	K$_2$CO$_3$, H$_2$O EtOH, rt	1200	99	[68]
NAS@Cu	CS$_2$CO$_3$, EtOH, 80 °C	120	97	[39]
Pd(II)-NHC complex	Cs$_2$CO$_3$, DMF, 100 °C	1440	99	[69]
NHC-Pd(II) complex	Cs$_2$CO$_3$, THF, 80 °C	720	88	[70]
Pd/Au NPs	K$_2$CO$_3$, EtOH/H$_2$O, 80 °C	1440	88	[71]
CA/Pd(0)	K$_2$CO$_3$, H$_2$O, 100 °C	120	94	[72]
Pd@SBA-15/ILDABCO	K$_2$CO$_3$, H$_2$O, 80 °C	90	97	[73]
BisPyP@ySiO$_2$@xSiO$_2$@NMP	Na$_2$CO$_3$, PEG, 70 °C	5	99	[This work]

Table 7. Comparison of the activity of Pd-BisPyP@bilayer-SiO$_2$@NMP in the reaction of iodobenzene and phenylboronic acid with other catalysts.

Data availability

The data that support the findings of this study are available on request from the corresponding author.

References

1. Kim, J. H., Park, J. S., Chung, H. W., Boote, B. W. & Lee, T. R. Palladium nanoshells coated with self-assembled monolayers and their catalytic properties. *RSC Adv.* **2**, 3968–3977 (2012).
2. Veisi, H., Hamelian, M. & Hemmati, S. Palladium anchored to SBA-15 functionalized with melamine-pyridine groups as a novel and efficient heterogeneous nanocatalyst for Suzuki–Miyaura coupling reactions. *Catal. A Chem.* **395**, 25–33 (2014).
3. Mohamed, M. G. *et al.* Construction hierarchically mesoporous/microporous materials based on block copolymer and covalent organic framework. *J. Taiwan Inst. Chem. Eng.* **112**, 180–192 (2020).
4. Kiani, M., Anaraki-Ardakani, H., Hasanzadeh, N. & Rayatzadeh, A. A novel magnetic nanocomposite (Fe$_3$O$_4$@ Saponin/Cr (III)) as a Potential recyclable catalyst for the synthesis of β-acetamidoketones derivatives. *Polycycl. Aromat. Compd.* **43**, 3670–3686 (2023).
5. Ghadamyari, Z., Shiri, A., Khojastehnezhad, A. & Seyedi, S. M. Zirconium (IV) porphyrin graphene oxide: A new and efficient catalyst for the synthesis of 3, 4-dihydropyrimidin-2 (1*H*)-ones. *Appl. Organomet. Chem.* **33**, e5091 (2019).
6. Allameh, S., Davoodnia, A. & Khojastehnezhad, A. An efficient and eco-friendly synthesis of 14-aryl-14*H*-dibenzo [a, j] xanthenes using H$_4$ [SiW$_{12}$O$_{40}$] as a heterogeneous and reusable catalyst under solvent-free conditions. *Chin. Chem. Lett.* **23**, 17–20 (2012).
7. Koli, R. R. *et al.* Gram bean extract-mediated synthesis of Fe$_3$O$_4$ nanoparticles for tuning the magneto-structural properties that influence the hyperthermia performance. *J. Taiwan Inst. Chem. Eng.* **95**, 357–368 (2019).
8. Rossi, L. M., Costa, N. J., Silva, F. P. & Wojcieszak, R. Magnetic nanomaterials in catalysis: Advanced catalysts for magnetic separation and beyond. *Green Chem.* **16**, 2906–2933 (2014).
9. Molaei Yielzoleh, F. & Nikoofar, K. Novel inorganic-bioorganic functionalized silica-magnetized core-shell (nano SO$_3$H-D-Leu@ SiO$_2$-Fe$_3$O$_4$) as reusable promoter for the synthesis of 7, 7'-((aryl) methylene) bis(N-cyclohexyl-2-(aryl)-6-methyl-3 H-imidazo [1, 2-b] pyrazol-3-imine) derivatives. *Polycycl. Aromat. Compd.* **42**, 3984–3999 (2022).
10. Ghadamyari, Z., Khojastehnezhad, A., Seyedi, S. M. & Shiri, A. Co (II)-porphyrin Immobilized on graphene oxide: An efficient catalyst for the beckmann rearrangement. *ChemistrySelect.* **4**, 10920–10927 (2019).
11. Khojastehnezhad, A., Moeinpour, F. & Javid, A. NiFe$_2$O$_4$@SiO$_2$–PPA nanoparticle: A green nanocatalyst for the synthesis of β-acetamido ketones. *Polycycl. Aromat. Compd.* **39**, 404–412 (2017).
12. Cui, X., Li, W., Ryabchuk, P., Junge, K. & Beller, M. Bridging homogeneous and heterogeneous catalysis by heterogeneous single-metal-site catalysts. *Nat. Catal.* **1**, c385-397 (2018).
13. Rahimizadeh, M. *et al.* Nanomagnetically modified ferric hydrogen sulfate (NiFe$_2$O$_4$@SiO$_2$-FHS): A reusable green catalyst for the synthesis of highly functionalized piperidine derivatives. *J. Iran. Chem. Soc.* **12**, 839–844 (2015).
14. Pang, L. L. *et al.* A novel detection method for DNA point mutation using QCM based on Fe$_3$O$_4$/Au core/shell nanoparticle and DNA ligase reaction. *Sens. Actuat.B* **127**, 311–316 (2007).
15. Ghorbani-Choghamarani, A., Tahmasbi, B., Noori, N. & Faryadi, S. Pd–S-methylisothiourea supported on magnetic nanoparticles as an efficient and reusable nanocatalyst for Heck and Suzuki reactions. *C. R. Chimie* **20**, 132–139 (2017).
16. Salviano, A. B. *et al.* Iron oxide nanoparticles supported on mesoporous MCM-41 for efficient adsorption of hazardous β-lactamic antibiotics. *Water Air Soil Pollut.* **229**, 1–14 (2018).
17. Najafi, M., Morsali, A. & Bozorgmehr, M. R. DFT study of SiO$_2$ nanoparticles as a drug delivery system: Structural and mechanistic aspects. *Struct. Chem.* **30**, 715–726 (2019).
18. Appaturi, J. N., Selvaraj, M. & Hamid, S. B. A. Synthesis of 3-(2-furylmethylene)-2, 4-pentanedione using DL-Alanine functionalized MCM-41 catalyst via Knoevenagel condensation reaction. *Micropor. Mesopor. Mater.* **260**, 260–269 (2018).
19. Zare, A. *et al.* Nano-2-(dimethylamino)-N-(silica-n-propyl)-N,N-dimethylethanaminium chloride as a novel basic catalyst for the efficient synthesis of pyrido [2, 3-d: 6, 5-d′] dipyrimidines. *New J. Chem.* **43**, 2247–2257 (2019).
20. Ghorbani-Choghamarani, A., Tahmasbi, B., Noori, N. & Faryadi, S. Pd–S-methylisothiourea supported on magnetic nanoparticles as an efficient and reusable nanocatalyst for Heck and Suzuki reactions. *C. R. Chim.* **20**, 132–139 (2017).
21. Nikoorazm, M., Ghorbani-Choghamaranai, A., Khanmoradi, M. & Moradi, P. Synthesis and characterization of Cu(II)-Adenine-MCM-41 as stable and efficient mesoporous catalyst for the synthesis of 5-substituted 1 H-tetrazoles and 1 H-indazolo [1, 2-b] phthalazine-triones. *J. Porous Mater.* **25**, 1831–1842 (2018).
22. Garkoti, C., Shabir, J. & Mozumdar, S. An imidazolium based ionic liquid supported on Fe$_3$O$_4$@SiO$_2$ nanoparticles as an efficient heterogeneous catalyst for N-formylation of amines. *New J. Chem.* **41**, 9291–9298 (2017).
23. Shabani, N. *et al.* 2-Aminoisoindoline-1, 3-dione-functionalized Fe$_3$O$_4$/chloro-silane core-shell nanoparticles as reusable catalyst: An efficient heterogeneous magnetic nanoparticles for synthesis of 4 H-pyran derivatives through multicomponent reaction. *Polycycl. Aromat. Compd.* **42**, 4561–4577 (2022).
24. Kohzadian, A. & Filian, H. Production and characterization of Fe$_3$O$_4$@ SiO$_2$@ TMEDA-Pd as a very effectual interphase catalyst for the rapid preparation of di-aryl sulfides and pyrido-dipyrimidines. *Silicon* **15**, 4539–4554 (2023).
25. Veisi, H., Ozturk, T., Karmakar, B., Tamoradi, T. & Hemmati, S. In situ decorated Pd NPs on chitosan-encapsulated Fe$_3$O$_4$/SiO$_2$-NH$_2$ as magnetic catalyst in Suzuki–Miyaura coupling and 4-nitrophenol reduction. *Carbohydr. Polym.* **235**, 115966 (2020).
26. Veisi, H., Tamoradi, T., Karmakar, B., Mohammadi, P. & Hemmati, S. In situ biogenic synthesis of Pd nanoparticles over reduced graphene oxide by using a plant extract (*Thymbra spicata*) and its catalytic evaluation towards cyanation of aryl halides. *Mater. Sci. Eng. C* **104**, 109919 (2019).
27. Tamoradi, T., Mousavi, S. M. & Mohammadi, M. Praseodymium (iii) anchored on CoFe$_2$ O$_4$ MNPs: An efficient heterogeneous magnetic nanocatalyst for one-pot, multi-component domino synthesis of polyhydroquinoline and 2,3-dihydroquinazolin-4 (1*H*)-one derivatives. *New J. Chem.* **44**, 3012–3020 (2020).
28. Kumar, A. *et al.* Solid-state reaction synthesis of nanoscale materials: Strategies and applications. *Chem. Rev.* **122**, 12748–12863 (2022).
29. Franzén, R. G. Recent advances in the preparation of heterocycles on solid support: A review of the literature. *J. Combin. Chem.* **2**, 195–214 (2000).
30. Hajipour, A. R. & Rafiee, F. Dimeric ortho-palladated complex of 2,3-dimethoxybenzaldehyde oxime catalyzed Suzuki–Miyaura cross-coupling reaction under microwave irradiation. *J. Iran. Chem. Soc.* **12**, 1177–1181 (2015).
31. Tahmasbi, B. & Ghorbani-Choghamarani, A. Pd (0)-Arg-boehmite: As reusable and efficient nanocatalyst in Suzuki and Heck reactions. *Catal. Lett.* **147**, 649–662 (2017).
32. Shabbir, S. *et al.* Pd nanoparticles on reverse phase silica gel as recyclable catalyst for Suzuki–Miyaura cross coupling reaction and hydrogenation in water. *J. Organometal. Chem.* **846**, 296–304 (2017).
33. Khojastehnezhad, A. *et al.* Size-dependent catalytic activity of palladium nanoparticles decorated on core-shell magnetic microporous organic networks. *ACS Appl. Nano Mater.* **6**, 17706–17717 (2023).

34. Ghiaci, M., Zarghani, M., Moeinpour, F. & Khojastehnezhad, A. Preparation, characterization and application of silica-supported palladium complex as a new and heterogeneous catalyst for Suzuki and Sonogashira reactions. *Appl. Organomet. Chem.* **28**, 589–594 (2014).
35. Ghiaci, M., Zarghani, M., Khojastehnezhad, A. & Moeinpour, F. Preparation, characterization and first application of silica supported palladium-N-heterocyclic carbene as a heterogeneous catalyst for C–C coupling reactions. *RSC Adv.* **4**, 15496–15501 (2014).
36. Sharma, R. K., Sharma, S., Dutta, S., Zboril, R. & Gawande, M. B. Silica-nanosphere-based organic–inorganic hybrid nanomaterials: synthesis, functionalization and applications in catalysis. *Green Chem.* **17**, 3207–3230 (2015).
37. Zheng, J. *et al.* In situ loading of gold nanoparticles on $Fe_3O_4@SiO_2$ magnetic nanocomposites and their high catalytic activity. *Nanoscale* **5**, 4894–4901 (2013).
38. Yang, Y. *et al.* Magnetically separable mesoporous silica-supported palladium nanoparticle-catalyzed selective hydrogenation of naphthalene to tetralin. *Appl. Organomet. Chem.* **33**, e5204 (2019).
39. Kohzadi, H. & Soleiman-Beigi, M. A recyclable heterogeneous nanocatalyst of copper-grafted natural asphalt sulfonate (NAS@ Cu): Characterization, synthesis and application in the Suzuki–Miyaura coupling reaction. *New J. Chem.* **44**, 12134–12142 (2020).
40. Tailor, S. B. *et al.* Revisiting claims of the iron-, cobalt-, nickel-, and copper-catalyzed suzuki biaryl cross-coupling of aryl halides with aryl boronic acids. *Organometallics* **38**, 1770–1777 (2019).
41. Fareghi-Alamdari, R., Golestanzadeh, M. & Bagheri, O. An efficient and recoverable palladium organocatalyst for Suzuki reaction in aqueous media. *Appl. Organomet. Chem.* **31**, e3698 (2017).
42. Park, J. C. *et al.* Facile synthesis of a high performance NiPd@ CMK-3 nanocatalyst for mild Suzuki–Miyaura coupling reactions. *ChemCatChem.* **11**, 991–996 (2019).
43. Do Kim, K., Kim, S. S., Choa, Y. H. & Kim, H. T. Formation and surface modification of Fe_3O_4 nanoparticles by co-precipitation and sol-gel method. *J. Ind. Eng. Chem* **13**, 1137–1141 (2007).
44. Buskes, M. J. & Blanco, M. J. Impact of cross-coupling reactions in drug discovery and development. *Molecules* **25**, 3493 (2020).
45. Alonso, F., Beletskaya, I. P. & Yus, M. Non-conventional methodologies for transition-metal catalysed carbon–carbon coupling: A critical overview. Part 2: The Suzuki reaction. *Tetrahedron* **64**, 3047–3101 (2008).
46. Bao, Z., Chan, W. & Yu, L. Synthesis of conjugated polymer by the stille coupling reaction. *Chem. Mater.* **5**, 2–3 (1993).
47. Kotha, S., Lahiri, K. & Kashinath, D. Recent applications of the Suzuki–Miyaura cross-coupling reaction in organic synthesis. *Tetrahedron* **58**, 9633–9695 (2002).
48. Heydari, N., Bikas, R., Siczek, M. & Lis, T. Green carbon–carbon homocoupling of terminal alkynes by a silica supported Cu(ii)-hydrazone coordination compound. *Dalton Trans.* **52**, 421–433 (2023).
49. Fu, Q. *et al.* Micro/nano multiscale reinforcing strategies toward extreme high-temperature applications: Take carbon/carbon composites and their coatings as the examples. *J. Mater. Sci. Technol.* **96**, 31–68 (2022).
50. Chowdhury, P., Sehitoglu, H. & Rateick, R. Damage tolerance of carbon–carbon composites in aerospace application. *Carbon* **126**, 382–393 (2018).
51. Esmaeilpour, M., Sardarian, A. R. & Javidi, J. Synthesis and characterization of Schiff base complex of Pd (II) supported on superparamagnetic $Fe_3O_4@SiO_2$ nanoparticles and its application as an efficient copper-and phosphine ligand-free recyclable catalyst for Sonogashira–Hagihara coupling reactions. *J. Organomet. Chem.* **749**, 233–240 (2018).
52. Ghorbani-Choghamarani, A., Tahmasbi, B., Hudson, R. H. & Heidari, A. Supported organometallic palladium catalyst into mesoporous channels of magnetic MCM-41 nanoparticles for phosphine-free CC coupling reactions. *Microporous Mesoporous Mater.* **284**, 366–377 (2019).
53. Zare, A., Sadeghi-Takallo, M., Karami, M. & Kohzadian, A. Synthesis, characterization and application of nano-N,N,N′,N′-tetramethyl-N-(silica-n-propyl)-N′-sulfo-ethane-1, 2-diaminium chloride as a highly efficient catalyst for the preparation of N,N′-alkylidene bisamides. *Res. Chem. Intermed.* **45**, 2999–3018 (2019).
54. Jazinizadeh, E., Zare, A., Sajadikhah, S. S., Barzegar, M. & Kohzadian, A. Synthesis, characterization and application of a magnetically separable nanocatalyst for the preparation of 4,4′-(arylmethylene)-bis (3-methyl-1-phenyl-1 H-pyrazol-5-ol) derivatives. *Res. Chem. Intermed.* **48**, 5059–5075 (2022).
55. Aphesteguy, J. C., Kurlyandskaya, G. V., De Celis, J. P., Safronov, A. P. & Schegoleva, N. N. Magnetite nanoparticles prepared by co-precipitation method in different conditions. *Mater. Chem. Phys.* **161**, 243–249 (2015).
56. Garole, V. J., Choudhary, B. C., Tetgure, S. R., Garole, D. J. & Borse, A. U. Palladium nanocatalyst: Green synthesis, characterization, and catalytic application. *Int. J. Environ. Sci. Technol* **16**, 7885–7892 (2019).
57. Briggs, B. D., Pekarek, R. T. & Knecht, M. R. Examination of transmetalation pathways and effects in aqueous Suzuki coupling using biomimetic Pd nanocatalysts. *J. Phys. Chem.* **118**, 18543–18553 (2014).
58. Peng, Y. Y., Liu, J., Lei, X. & Yin, Z. Room-temperature highly efficient Suzuki–Miyaura reactions in water in the presence of Stilbazo. *Green Chem.* **12**(6), 1072–1075 (2010).
59. Ghorbani-Choghamarani, A. & Norouzi, M. Palladium supported on modified magnetic nanoparticles: A phosphine-free and heterogeneous catalyst for Suzuki and Stille reactions. *Appl. Organometal. Chem.* **30**, 140–147 (2016).
60. Bai, L. & Wang, J. X. Reusable, polymer-supported, palladium-catalyzed, atom-efficient coupling reaction of aryl halides with sodium tetraphenylborate in water by focused microwave irradiation. *Adv. Synth. Catal.* **350**, 315–320 (2008).
61. Samarasimhareddy, M., Prabhu, G., Vishwanatha, T. M. & Sureshbabu, V. V. PVC-supported palladium nanoparticles: An efficient catalyst for Suzuki cross-coupling reactions at room temperature. *Synthesis* **45**, 1201–1206 (2013).
62. Modak, A., Mondal, J., Sasidharan, M. & Bhaumik, A. Triazine functionalized ordered mesoporous polymer: a novel solid support for Pd-mediated C–C cross-coupling reactions in water. *Green Chem.* **13**, 1317–1331 (2011).
63. Orgiu, E., Crivillers, N., Rotzler, J., Mayor, M. & Samorì, P. Tuning the charge injection of P3HT-based organic thin-film transistors through electrode functionalization with oligophenylene SAMs. *J. Mater. Chem.* **20**, 10798–10800 (2010).
64. Emmanuvel, L. & Sudalai, A. Phosphine ligand and base-free, Pd-catalyzed oxidative cross-coupling reaction of arylboronic acids with arylmercuric acetates. *Arkivoc* **14**, 126–133 (2007).
65. Nikoorazm, M., Ghorbani-Choghamarani, A., Noori, N. & Tahmasbi, B. Palladium 2-mercapto-N-propylacetamide complex anchored onto MCM-41 as efficient and reusable nanocatalyst for Suzuki, Stille and Heck reactions and amination of aryl halides. *Appl. Organometal. Chem.* **30**, 843–851 (2016).
66. Filian, H., Ghorbani-Choghamarani, A. & Tahanpesar, E. Pd (0)-guanidine@ MCM-41 as efficient and reusable heterogeneous catalyst for C–C coupling reactions. *J. Porous Mater.* **26**, 1091–1101 (2019).
67. Karimi, B., Mansouri, F. & Vali, H. highly water-dispersible/magnetically separable palladium catalyst based on a $Fe_3O_4@SiO_2$ anchored TEG-imidazolium ionic liquid for the Suzuki–Miyaura coupling reaction in water. *Green Chem.* **16**, 2587–2596 (2014).
68. Li, S., Lin, Y., Cao, J. & Zhang, S. Guanidine/Pd (OAc) 2-catalyzed room temperature Suzuki cross-coupling reaction in aqueous media under aerobic conditions. *J. Org. Chem.* **72**, 4067–4072 (2007).
69. Xu, Q., Duan, W. L., Lei, Z. Y., Zhu, Z. B. & Shi, M. A novel cis-chelated Pd (II)–NHC complex for catalyzing Suzuki and Heck-type cross-coupling reactions. *Tetrahedron* **61**, 11225–11229 (2005).
70. Chen, T., Gao, J. & Shi, M. A novel tridentate NHC–Pd (II) complex and its application in the Suzuki and Heck-type cross-coupling reactions. *Tetrahedron* **62**, 6289–6294 (2006).
71. Nasrollahzadeh, M., Azarian, A., Maham, M. & Ehsani, A. Synthesis of Au/Pd bimetallic nanoparticles and their application in the Suzuki coupling reaction. *J. Ind. Eng. Chem.* **21**, 746–748 (2006).

72. Faria, V. W. *et al.* Palladium nanoparticles supported in a polymeric membrane: an efficient phosphine-free "green" catalyst for Suzuki–Miyaura reactions in water. *RSC Adv.* **4**, 13446–13452 (2014).

73. Rostamnia, S., Doustkhah, E. & Zeynizadeh, B. Cationic modification of SBA-15 pore walls for Pd supporting: Pd@ SBA-15/ILDABCO as a catalyst for Suzuki coupling in water medium. *Micropor. Mesopor. Mater.* **222**, 87–93 (2016).

Acknowledgements

Author contributions

E.A.A: prepared some Suzuki reaction products (1a-8a), and assisting to edit the article. H.K.M: prepared some Suzuki reaction products (9a-16a). D.K.V: prepared some Stille reaction products (1b-5b). S.K.J: prepared some Stille reaction products (6b-10b). E.A.M.S: Optimized Stille reaction. A.H.K: Optimized Suzuki reaction. A.K: characterized the structure of the catalyst by SEM, TEM and EDS analyzes. A.A: characterized the structure of the catalyst via ICP, VSM and BET analyzes. A.A: characterized the structure of the catalyst through XRD and TGA analyzes. R.F: prepared the catalyst, and writing the article. We have confirmed.

Funding

Competing interests

The authors declare no competing interests.

Additional information

Correspondence and requests for materials should be addressed to R.F.

Reprints and permissions information is available at www.nature.com/reprints.

Publisher's note Springer Nature remains neutral with regard to jurisdictional claims in published maps and institutional affiliations.